

Reduction of Fiber Chromatic Dispersion Effects in Fiber-Wireless and Photonic Time-Stretching System Using Polymer Modulators

Jeehoon Han, *Student Member, IEEE*, Byoung-Joon Seo, *Student Member, IEEE*, Yan Han, Bahram Jalali, and Harold R. Fetterman, *Fellow, IEEE, Fellow, OSA*

Abstract—We have investigated the general characteristics of the power penalty due to the fiber chromatic dispersion effects in both fiber-wireless and photonic time-stretching systems. Two different modulation schemes have been demonstrated to reduce this penalty using our novel polymer modulators incorporating a multi-mode interference (MMI) structure. A single-sideband (SSB) modulator configuration has almost completely eliminated this penalty without a bandwidth limit. A double-sideband (DSB) modulator configuration with an appropriate quadrature bias has also shown significant improvement in bandwidth limitations for a given fiber link length.

Index Terms—Fiber-wireless systems, photonic time-stretching, polymer modulators, power penalty, single-sideband modulation.

I. INTRODUCTION

IN FIBER-WIRELESS systems, the radio frequency (RF) signals are generated at the central exchange using optical techniques and transmitted to the remote base stations over optical fiber links. The simplest and best technique to modulate optical fields with RF signals is an intensity modulation scheme via Mach-Zehnder modulators (MZMs) with continuous-wave (CW) lasers. Using the conventional DSB modulation scheme, the RF power detected at the base station suffers from a periodic degradation due to the fiber chromatic dispersion. As the RF frequency or fiber-link distance increases, this effect is even more severe and limits the system performance. This detrimental effect can be mitigated using alternative modulation schemes [1]–[3]. In this paper, we derive more specific and standard expressions and confirmed them by experiments using standard MZM designs. This examination of the power penalty in CW applications can be also utilized for the appropriate and clear understanding of those in pulsed applications.

Photonic time-stretching (PTS) utilizes optical systems to enable high-speed analog-to-digital conversion (ADC) of RF signals at otherwise inaccessible high frequencies. By exploiting chirped optical pulses and chromatic dispersion in standard optical fibers, high-frequency RF signals can be stretched in time, without distortion, to lower frequency regimes where conventional electronic ADCs are able to digitize with high resolution. However, as in CW applications, the inherent fiber chromatic

dispersion effects limit the actual bandwidth of PTS system [4]–[6]. We describe the general theory and present for the first time the experimental demonstration of PTS system associated with various modulation conditions including SSB modulation.

II. POWER PENALTY IN FIBER-WIRELESS SYSTEM

The basic structure for these MZMs is shown in Fig. 1 representing all possible modulation schemes and biases. If the input optical signal at Ω is $E_{in}(t) = e^{i\Omega t}$ with unit magnitude, the generalized expression for output optical field from MZM modulated at ω_m is given by

$$E(t) = \frac{1}{2} e^{i\Omega t} \left\{ e^{i\Delta_1 \cos(\omega_m t + \theta)} + e^{i\Delta_2 \cos(\omega_m t) + i\phi_b} \right\} \quad (1)$$

where $\Delta_i = \pi V_i / V_\pi$ is the modulation depth at i arm, $\phi_b = \pi V_b / V_\pi$ is the optical phase shift controlled by dc bias, V_π is the half-wave voltage. When this signal travels through the standard fiber with length of L , the resulting optical field can be written in terms of three frequency components, Ω , $\Omega - \omega_m$ and $\Omega + \omega_m$, with different phase changes due to the chromatic dispersion

$$E(t, L) = \frac{1}{2} \left\{ [J_0(\Delta_1) + J_0(\Delta_2) e^{i\phi_b}] e^{i\Omega t} e^{-i\varphi_\Omega} + i [J_1(\Delta_1) e^{-i\theta} + J_1(\Delta_2) e^{i\phi_b}] \times e^{i(\Omega - \omega_m)t} e^{-i\varphi_{\Omega - \omega_m}} + i [J_1(\Delta_1) e^{i\theta} + J_1(\Delta_2) e^{i\phi_b}] \times e^{i(\Omega + \omega_m)t} e^{-i\varphi_{\Omega + \omega_m}} \right\} \quad (2)$$

where $J_0(\Delta_1)$, $J_0(\Delta_2)$, $J_1(\Delta_1)$, $J_1(\Delta_2)$ are the Bessel function values and Δ is assumed to be small. Each phase change can be specified by usual Taylor expansion of the propagation constants $\beta(\omega)$

$$\begin{aligned} \varphi_\Omega &= \beta(\Omega)L \\ \varphi_{\Omega - \omega_m} &= \beta(\Omega)L - \beta'(\Omega)L\omega_m + \frac{1}{2}\beta''(\Omega)L\omega_m^2 \\ \varphi_{\Omega + \omega_m} &= \beta(\Omega)L + \beta'(\Omega)L\omega_m + \frac{1}{2}\beta''(\Omega)L\omega_m^2 \end{aligned} \quad (3)$$

where group velocity dispersion in standard fibers is defined by $D_\lambda = |2\pi c\beta''/\lambda_0^2| = 17 \text{ ps/km} \cdot \text{nm}$.

At the photodiode, the RF signal at modulation frequency is produced as a result of interference among these components. Normally the detected RF power is associated with their phase

Manuscript received October 11, 2002; revised February 27, 2003. This work was supported in part by AFOSR and DARPA.

The authors are with the Electrical Engineering Department, University of California, Los Angeles, CA 90095 USA (e-mail: hoon@ee.ucla.edu).

Digital Object Identifier 10.1109/JLT.2003.812155

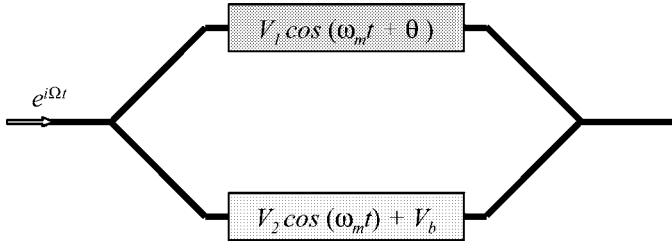


Fig. 1. The general schematic for MZM structure representing all possible modulation schemes and bias conditions.

relationship, which consequently is a strong function of the dispersion parameter, fiber length and modulation frequency as can be seen in (3). In the following sections, it will be shown that it also could be significantly affected by modulation schemes and bias conditions.

A. Push-Pull DSB Modulation ($\Delta_1 = \Delta_2 = \Delta$, $\theta = \pi$)

Both arms are driven by RF signals with equal power and out of phase by π . One arm is biased either at V_{+b} or V_{-b} corresponding to the quadrature bias voltages on the positive or negative slope of the MZM transfer function such that $\phi_{+b} = \pi V_{+b}/V_\pi = \pi/2$, $\phi_{-b} = \pi V_{-b}/V_\pi = -\pi/2$ with respect to the other arm. This is so called push-pull operation and the optical field from the MZM can be expressed by

$$E(t) = \frac{1}{2} e^{i\Omega t} \left\{ e^{-i\Delta \cos(\omega_m t)} \pm i e^{i\Delta \cos(\omega_m t)} \right\} \quad (4)$$

The resulting intensity at the modulation frequency after propagating through fiber of length L is

$$I_{\omega_m}(t) \propto J_0 J_1 \cos \left(\frac{\beta'' L \omega_m^2}{2} \right) \cos(\omega_m t - \beta' L \omega_m). \quad (5)$$

An optical carrier and two sidebands generated by DSB modulation experience different phase shifts along the fiber and result in a relative phase difference between the carrier and each sideband. Due to this effect, the RF power detected at the modulation frequency is not constant but varies with their phase relationship, which is dependent on dispersion parameter, fiber length, and modulation frequency. This power penalty is represented by the first cosine term in (5). Since, in this case, both RF arms are balanced, there is no initial phase difference between carrier and each sideband at the MZM so that the power variation appears in the form of $\cos((\beta'' L \omega_m^2)/2)$ for both quadrature biases.

B. Single-Arm DSB Modulation ($\Delta_1 = 0$, $\Delta_2 = \Delta$)

When only one of arms is modulated and biased at $V_{\pm b}$, the optical field from the MZM can be expressed by

$$E(t) = \frac{1}{2} e^{i\Omega t} \left\{ 1 \pm i e^{i\Delta \cos(\omega_m t)} \right\} \quad (6)$$

The resulting intensity at ω_m after propagating through fiber of length L is

$$I_{\omega_m}(t) \propto J_0 J_1 \cos \left(\frac{\beta'' L \omega_m^2}{2} \pm \frac{\pi}{4} \right) \cos(\omega_m t - \beta' L \omega_m). \quad (7)$$

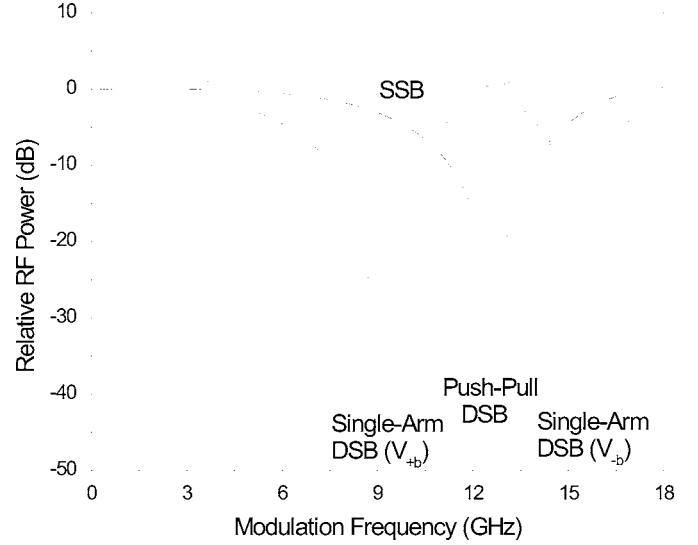


Fig. 2. Power penalty as a function of modulation frequencies in CW system with different modulation schemes and quadrature biases for length of 23 km.

Similar to the previous push-pull operation case, the detected RF power is varying with the cosine function (first cosine term) due to the same effect. However, in this case, this modulation scheme introduces the additional phase difference between the carrier and each sideband at the MZM, which influences the detected RF power. As shown in (7), the first cosine term is shifted by $\pm\pi/4$ when the signs correspond to quadrature bias voltages, $V_{\pm b}$. This indicates that the power nulls for the two different quadrature biases appear at different modulation frequencies (or fiber lengths). The DSB modulation driven in this fashion can increase the bandwidth for a given fiber link length or vice versa.

Fig. 2 shows the theoretical graph for the power penalty as a function of modulation frequencies resulting from the two DSB modulation schemes discussed above. Push-pull operation has only one power null while single-arm operation has two depending on the quadrature bias points as shown in Fig. 2. It can be also seen that single-arm operation biased at V_{-b} provides enhanced bandwidth compared to other two modulation schemes. On the other hand, even though the same modulation scheme is applied, the bandwidth is degraded by a factor of $\sqrt{3}$ when biased at V_{+b} .

C. SSB Modulation ($\Delta_1 = \Delta_2 = \Delta$, $\theta = \pm\pi/2$)

When the both arms are modulated but the RF phase difference on the two arms is $\pm\pi/2$, with quadrature bias voltage $V_{\pm b}$, the optical field from the MZM becomes

$$E(t) = \frac{1}{2} e^{i\Omega t} \left\{ e^{\mp i\Delta \sin(\omega_m t)} \pm i e^{i\Delta \cos(\omega_m t)} \right\}. \quad (8)$$

The resulting intensity at ω_m after propagating through fiber L is

$$I_{\omega_m}(t) \propto J_0 J_1 \sin \left(\omega_m t - \beta' L \omega_m \pm \frac{\pi}{4} \right). \quad (9)$$

The SSB modulation cancels out one of the sidebands and generates only one sideband with a carrier. As a consequence, it is seen in (9) that the first cosine term associated with the power penalty disappears so that detected RF power is constant.

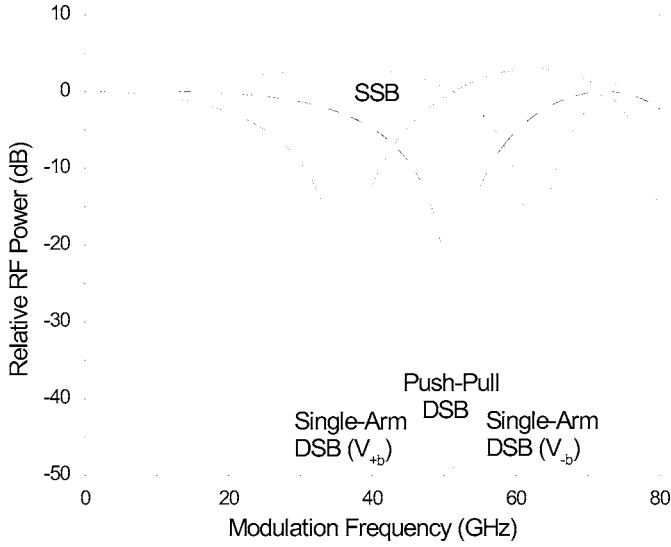


Fig. 3. Theoretical power penalty in PTS system with various modulation schemes and quadrature biases for $M = 10$.

Ideally, the RF signal generated by SSB modulation does not suffer from bandwidth or fiber link length limitations with either quadrature bias (see Fig. 2).

III. POWER PENALTY IN TIME-STRETCHING SYSTEM

PTS systems exploit the group velocity dispersion to temporally expand a pulse while preserving its envelope shape which has information. The details of this theory are described in [4]–[6]. Instead of the plane waveform in the CW case, a transform limited Gaussian pulse is assumed such as

$$E_{\text{source}}(t) = \exp\left(-\frac{t^2}{\tau^2}\right) \exp(i\Omega t). \quad (10)$$

Then, the same principle as in the CW system is applied to the PTS system so that the resulting intensity at ω_m for each modulation scheme is

$$I_{\omega_m}(t) \propto \cos\left(\frac{\beta'' L_2 \omega_m^2}{2M}\right): \text{push-pull DSB with } V_{\pm b} \quad (11)$$

$$I_{\omega_m}(t) \propto \cos\left(\frac{\beta'' L_2 \omega_m^2}{2M} \pm \frac{\pi}{4}\right): \text{single-arm DSB with } V_{\pm b} \quad (12)$$

$$I_{\omega_m}(t) = \text{const} : \text{SSB with } V_{\pm b} \quad (13)$$

where a stretching factor $M = 1 + (L_2/L_1)$.

Fig. 3 shows the theoretical graph for the power penalty as a function of modulation frequencies in a PTS system with $M = 10$. In the SSB modulation, the cosine term associated with power penalty disappears so that detected RF power is constant and does not suffer from bandwidth or fiber link length limitations with either quadrature bias. As in the CW case, push-pull operation has only one power null while single-arm operation has two depending on the quadrature bias points. For example, when the PTS system incorporates either SSB modulation or single-arm DSB modulation biased at V_{-b} , RF signals of up to 40 GHz (which is attainable by current technology) can be stretched out up to 4 GHz with $M = 10$ without suffering from the power penalty. On the other hand, the power degradation is

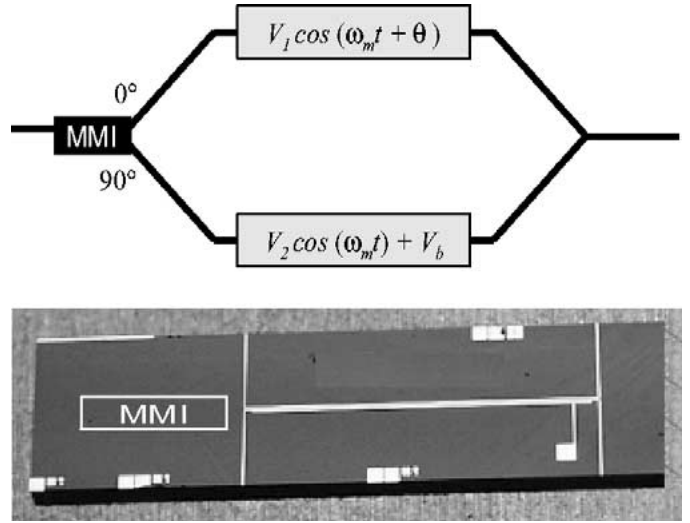


Fig. 4. MZMs incorporating MMI couplers and devices fabricated with polymer material, CPW1/APC.

severe for push-pull operation or single-arm operation biased at V_{+b} in this modulation frequency range.

IV. DEVICE FABRICATION AND EXPERIMENTAL SETUP

The SSB MZM structure in Fig. 4 was fabricated using the recently developed polymer materials (CPW1/APC) and advanced polymer fabrication technologies. This guest-host system exhibits a high EO coefficient, low material loss at $1.55 \mu\text{m}$, and wideband frequency response over 100 GHz [7]. The single mode (SM) ridge optical waveguides were fabricated using the new inverted rib structures [8]. The key benefit of these inverted rib structures is that it can eliminate the damage problem on the core layer by the photoresist solvents when the waveguides are defined in the core layer. This ultimately resulted in much simpler fabrication procedure and lower propagation losses. Also the SM waveguide structures were designed to provide the symmetric mode shape with a rib depth of $0.8 \mu\text{m}$ and waveguide width of $4 \mu\text{m}$. A large optical nonlinearity in the core region was achieved through electrode poling. The microstrip lines were vertically aligned to the optical waveguides in the interaction regions to provide inherent velocity match of RF signal and optical signal.

In order to reduce the complexity and bias drift from applying additional DC bias, instead of using a normal Y-junction splitting structure, an asymmetrical 1-by-2 MMI coupler was used in front of the SSB modulator. This structure was intended to offer the built-in bias with the equal power and required optical phase shifts of $\pi/2$ for two arms. The measured excess loss due to the MMI was less than 1 dB and power difference at two outputs was less than 0.1 dB, which corresponds to the phase difference less than 1° .

Fig. 5 shows the experimental setup for the PTS system (and CW system). The optical source is a passively mode-locked Er^{3+} fiber pulse laser with a 40 nm bandwidth at $1.55 \mu\text{m}$ and a 40 MHz repetition rate ($1.55 \mu\text{m}$ Er^{3+} fiber CW laser for CW system). Both fiber spools L_1 and L_2 are standard SMF ($L_1 = 0$, $L_2 = 23 \text{ km}$ for CW system). The dispersed input optical signal from L_1 is modulated at MZM by a 20 GHz sweep

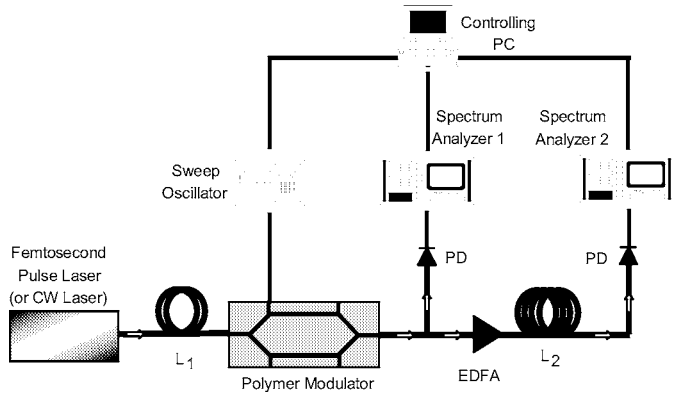


Fig. 5. Block diagram of experimental setup for PTS system (or CW system).

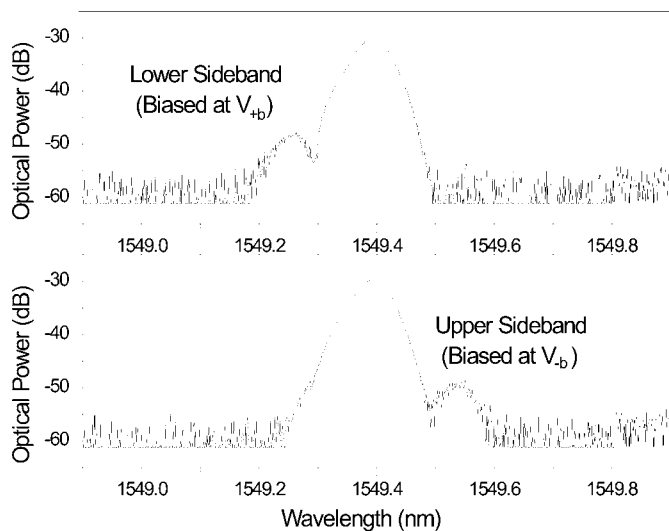


Fig. 6. Measured optical output SSB spectrums on OSA at a modulation frequency of 18 GHz.

oscillator and amplified in an EDFA before entering L_2 . The stretched output from L_2 spool is detected by a photodiode and amplified by a RF amplifier. To exclude the frequency response of the MZM, the difference of the RF power before and after L_2 is measured by two RF spectrum analyzers.

V. EXPERIMENTAL RESULTS

A. Measurement in CW System

The SSB modulation at 18 GHz with a CW laser was first confirmed on the optical spectrum analyzer (OSA) at both quadrature bias voltages $V_{\pm b}$ to ensure the performance of our SSB modulators (Fig. 6). The upper sideband spectrum is corresponding to the quadrature bias at V_{-b} , and lower upper sideband spectrum is corresponding to the quadrature bias at V_{+b} .

Fig. 7 shows the measured power penalty for the various modulation schemes and two quadrature bias points when the fiber length is 23 km. For the SSB modulation, the power nulls have not been observed for the entire frequency range at both quadrature bias points. On the other hand, the DSB modulation driven by single-arm operation has different power nulls depending on

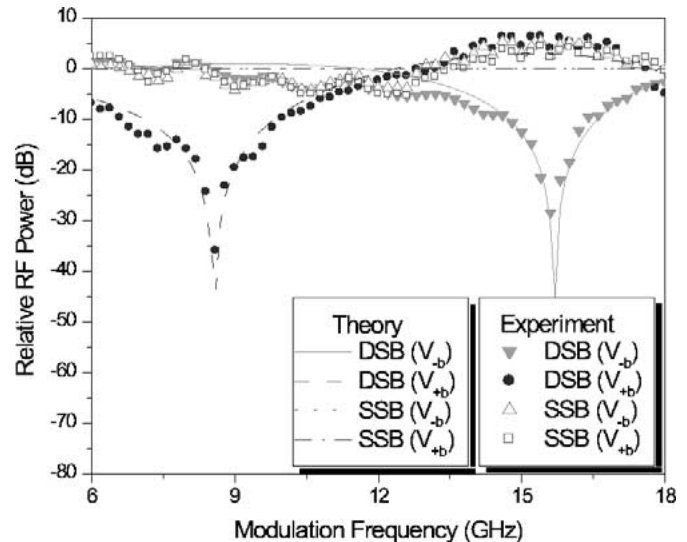


Fig. 7. Measured power penalty in CW system for various modulation schemes and quadrature biases ($L = 23$ km).

the quadrature bias points. The bandwidth, when biased at V_{-b} , has been increased by an amount of $\sqrt{3}$ compared to the other quadrature bias point as can be seen in (7). The measured power nulls corresponding to V_{+b} and V_{-b} appear at 8.6 GHz and 15.6 GHz, respectively, slightly deviates from the expected values from (7) by approximately 0.5 GHz. This can be caused by factors such as an uneven splitting ratio, the modulation depth and small deviations from the quadrature bias points. These factors cause a small change in the initial phase which can slightly move the positions of the power nulls. The theoretical plot in Fig. 7 is calculated assuming a splitting ratio of 1, a negligible modulation depth ($J_0 = 1$) and a deviation from the quadrature bias of $0.3 V$.

B. Measurement in PTS System

In our PTS measurement, the RF signal of up to 18 GHz was stretched out to 8.6 GHz ($M = 2.1$). At each modulation frequency, the center of the shifted RF spectrum is observed on the spectrum analyzer. Fig. 8 shows the measured output RF frequencies as a function of modulation frequencies with fiber spools, $L_1 = 13.5$ km and $L_2 = 15$ km, which is in good agreement with the theoretical value for all modulation schemes and bias conditions. A low M factor of 2.1 was intentionally used in our experiment to be able to see the first power nulls resulting from the DSB modulation biased at $V_{\pm b}$ below 20 GHz frequency range. Since the frequency values at power nulls are proportional to \sqrt{M} , the first power nulls for the M greater than 2 appear far beyond this frequency range.

The measured RF power penalties as a function of modulation frequency for the various modulation conditions are shown in Fig. 9. Also shown in Fig. 9 are the theoretical power penalties including the effects described in the CW case such as a splitting ratio of 0.95, a negligible modulation depth ($J_0 = 1$) and a deviation from the quadrature bias of $1.3 V$. The deviation from the original theoretical plot without considering these effects is about 2.5 GHz.

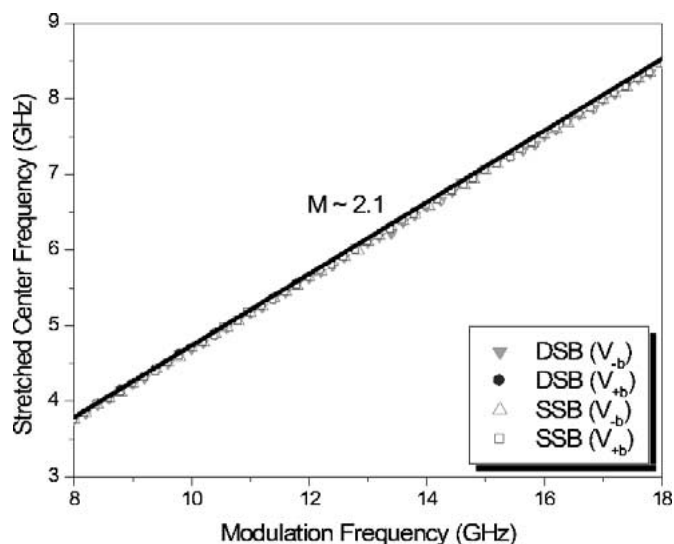


Fig. 8. Measured time stretch ratio for DSB and SSB modulation with different quadrature biases.

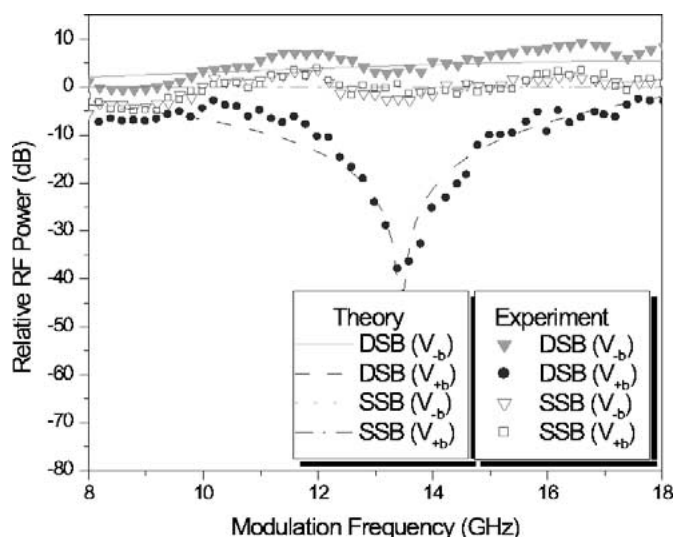


Fig. 9. Measured power penalty in PTS system for various modulation schemes and quadrature biases.

The DSB modulation biased at V_{+b} shows the first power null at around 13.5 GHz while the DSB modulation biased at V_{-b} is expected to appear at 28 GHz. Therefore, the limit on the modulation frequency can be significantly improved even for the DSB modulation by using the alternative quadrature bias point. On the other hand, the SSB modulation, for both quadrature bias points, almost completely eliminates this penalty effect without a bandwidth limit as shown in Fig. 9.

Fig. 10 shows the RF power spectral density of modulated pulse before and after stretching for the DSB modulation with two quadrature bias points, $V_{\pm b}$, at the modulation frequency of 13.5 GHz. As expected from Fig. 9, the stretched RF signals at this modulation frequency exhibit considerable amount of power at quadrature bias point V_{-b} and almost zero power at quadrature bias point V_{+b} .

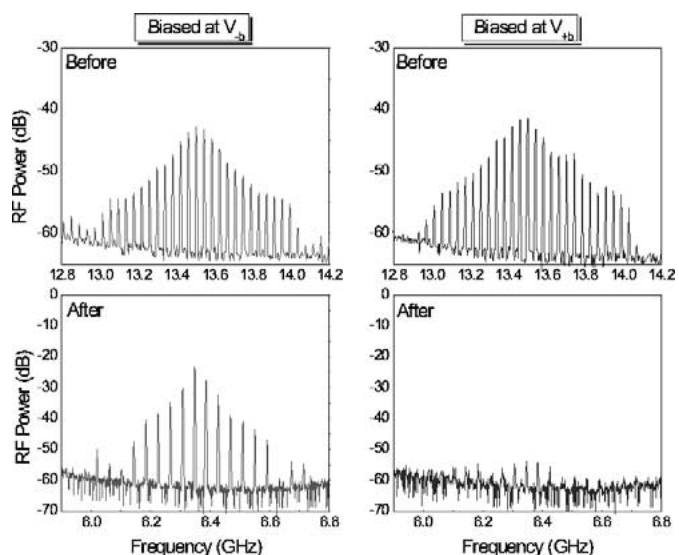


Fig. 10. RF power spectral density of modulated pulse before and after stretching for DSB modulation at two quadrature bias points. The spacing between peaks corresponds to the repetition rate of the mode-locked laser.

VI. CONCLUSION

In both fiber wireless and photonic time-stretching system, the power penalty due to the fiber chromatic dispersion effects is undesirable and limits the system performance. We have demonstrated techniques to reduce this power penalty using both polymer-based SSB and DSB modulators. The limit on the modulation frequency due to this penalty can be almost completely eliminated with the SSB modulation without a bandwidth limitation and also can be significantly improved with the DSB modulation by using an alternative quadrature bias point. These results indicate that SSB modulation or appropriately biased DSB modulation can have important roles in both CW and pulsed applications.

REFERENCES

- [1] A. Gnauck, S. Korothy, J. Veselka, J. Nagel, and D. Moser, "Dispersion penalty reduction using an optical modulator with adjustable chirp," *IEEE Photon. Technol. Lett.*, vol. 3, pp. 916–918, Oct. 1991.
- [2] F. Devaux, Y. Sorel, and J. Kerdiles, "Simple measurement of fiber dispersion and of chirp parameter of intensity modulated light emitter," *J. Lightwave Technol.*, vol. 11, pp. 1937–1940, Dec. 1993.
- [3] G. Smith, D. Novak, and Z. Ahmed, "Overcoming chromatic-dispersion effects in fiber-wireless systems incorporating external modulators," *IEEE Trans. Microwave Theory Tech.*, vol. 45, pp. 1410–1415, Aug. 1997.
- [4] F. Coppinger, A. Bhushan, and B. Jalali, "Photonic time stretch and its application to analog-to-digital conversion," *IEEE Trans. Microwave Theory Tech.*, vol. 47, pp. 1309–1314, July 1999.
- [5] D. Chang, H. Erlig, M. Oh, C. Zhang, W. Steier, L. Dalton, and H. Fetterman, "Time stretching of 102-GHz millimeter waves using novel 1.55 μm polymer electrooptic modulator," *IEEE Photon. Technol. Lett.*, vol. 12, pp. 537–539, May 2000.
- [6] J. Fuster, "Single-sideband modulation in photonic time-stretch analog-to-digital conversion," *Electron. Lett.*, vol. 37, no. 1, pp. 67–68, Jan 2001.
- [7] M. Oh, H. Zhang, C. Zhang, H. Erlig, Y. Chang, B. Tsap, D. Chang, A. Szep, W. Steier, H. Fetterman, and L. R. Dalton, "Recent advances in electrooptic polymer modulators incorporating highly nonlinear chromophore," *IEEE J. Select. Topics Quantum Electron.*, vol. 7, pp. 826–835, Sept./Oct. 2000.
- [8] S. Kim, H. Zhang, D. Chang, C. Zhang, C. Wang, W. Steier, and H. Fetterman, "Electrooptic polymer modulators with an inverted-rib waveguide structure," *IEEE Photon. Technol. Lett.*, vol. 15, pp. 218–220, Feb. 2003.



Jeehoon Han (S'01) received the B.S. degree in physics from the Chonbuk National University, Chonju, South Korea, in 1996 and the M.S. degree in electrical engineering from the University of Florida, Gainesville, in 1998, working on the fabrication of semiconductor laser devices. He is currently pursuing the Ph.D. degree in electrical engineering at the University of California, Los Angeles.

His current research is in the area of optoelectronic devices and optical communications using millimeter waves.



Byoung-Joon Seo (S'03) received the B.S. degree in electrical engineering from Seoul National University, Seoul, Korea, in 1998 and worked for Woori Technology in Seoul, from 1998 to 2001. He is currently pursuing the M.S. degree at the University of California, Los Angeles.

Yan Han received the B.S. and M.S. degrees in electronic engineering from the Tsinghua University at Beijing, China, in 1998 and 2000, respectively. He is currently a doctoral candidate in the Department of Electrical Engineering at the University of California, Los Angeles.

His research interests include the areas of microwave photonic systems, optical communication systems, wireless communication systems, optical amplifiers, and fiber optics.

Bahram Jalali is a Professor of Electrical Engineering, the Director of the DARPA Center for Optical A/D System Technology (COAST) and the Director of the Optoelectronic Circuits and System Laboratory at University of California, Los Angeles (UCLA).

From 1988 to 1992, he was a Member of Technical Staff at the Physics Research Division of AT&T Bell Laboratories in Murray Hill, NJ, where he conducted research on ultrafast electronics and optoelectronics. He was responsible for successful development and delivery of 10 Gb/s lightwave circuits to U.S. Air Force in 1992. His current research interests are in microwave photonics, integrated optics, and fiber-optic ICs. He has over 100 publications and holds five U.S. patents. He is a member of the California Nano Sciences Institute (CNSI) and serves on the Advisory Board of the Discovery Center for Science and Technology, a southern California nonprofit organization. While on leave from UCLA from 1999 to 2001, he founded Cognet Microsystems, a Los Angeles-based fiber-optic component company. He served as Cognet's President, CEO, and Chairman, until the company's acquisition by Intel Corporation in April 2001.

Dr. Jalali was awarded the BridgeGate 20 Award in recognition of his contributions to the southern California high tech economy.

Harold R. Fetterman (SM'81-F'90) received the B.A. degree with honors from Brandeis University, Waltham, MA, and the Ph.D. degree in physics from Cornell University, Ithaca, NY, in 1962 and 1968, respectively.

Dr. Fetterman joined Lincoln Laboratory, Lexington, MA, in 1969, where his initial research concentrated on the use of submillimeter sources for spectroscopy. Since leaving Lincoln Laboratory, he has devoted his efforts to investigating new solid-state devices. During this period, he was one of the founders of the highly respected Millitech Corporation. In 1982, he joined the University of California, Los Angeles (UCLA), Electrical Engineering Department as a Professor and served as the first Director of the Center for High Frequency Electronics. From 1986 to 1989, he was Associate Dean for Research in the School of Engineering. Currently, he has programs in investigating new millimeter wave device concepts and novel means of high frequency testing using laser techniques. He has concentrated on combining high frequency structures and systems with optical devices. These efforts include CW optical mixing experiments using three terminal devices, high-speed polymer optical modulators and traveling wave photodetectors which are now being extended to over 200 GHz.

Dr. Fetterman is a Fellow of the Optical Society of America (OSA) and is currently the Chair of the Executive Committee of the Henry Samueli School of Engineering and Applied Science at UCLA.